

Detachment control in KSTAR with Tungsten divertor

Anchal Gupta^{a,*}, David Eldon^b, KyuBeen Kwon^a, Anthony Leonard^b, Xueqiao Xu^c, Menglong Zhao^c, Ben Zhu^c

^a*Oak Ridge Associated Universities, 100 ORAU Way, Oak Ridge, TN 37830, USA*

^b*General Atomics, 3550 General Atomics Ct., San Diego, CA 92121, USA*

^c*Lawrence Livermore National Laboratory, PO Box 808, Livermore, CA 94550, USA*

Abstract

We have demonstrated detachment control in KSTAR with the new Tungsten divertor using two different control variables. First variable is the attachment friction calculated from 2-Point Model (2PM) using the ion saturation current density from divertor langmuir probes. Second, we used a prototype neural network surrogate model of UEDGE 2D trained on a set of about 70,000 simulations to provide a realtime estimate of heat flux at the outer divertor. We present the successful detachment control results and discuss future improvements in the control infrastructure and control variables for future burning plasma experiments.

1. Introduction

Burning plasma tokamaks such as ITER[1], SPARC[2], and the various DEMO concepts are estimated to exhaust very high heat flux in the Scrape-off Layer (SOL) towards the divertor target. As part of the very hot core plasma escapes the magnetic confinement withing the last closed flux surface, the hot ions rapidly travel along the open field lines in SOL region towards the divertor targets. To withstand the high heat flux, the divertor target plates are planned to be made out of tungsten which has high strength and the higest melting point of any metal. However, tungsten being a very high-Z material posses contamination challenges for the core plasma and it is important to develop operation stategies that limit the tungsten sputtering, especially in the divertor region where hot plasma interacts with the tungsten surface in a very narrow region of the order of a few mm[3]. Thus, experimental reactors such as KSTAR are in the process of upgrading their divertor and vessel walls to tungsten to design control systems and perform plasma studies in the presence of tungsten contamination.

It is estimated that for steady state operation, the constant heat flux reaching the divertor plates has to be below 10-15 MW/m²[4] to avoid surface metling and structural damage to the divertor plates. Additionally, the electron temperature at the target plate must be below 8 eV[5] to avoid sputtering of tungsten and subsequent contamination of the core plasma. The heat flux reaching the divertor is typically reduced by puffing in gas in the SOL region to dissipate energy and momentum from the exhaust plasma through ionization, charge exchange, and radiation. As the puffed gas neutrals travel towards the core plasma, they radiate energy based on local electron temperature and density. At higher temperatures, more and more electrons get stripped away from the neutral atoms and the raidation reduces and the main dissipation mechanism becomes charge exchange

and ionization. Thus for effective and fast cooling, impurity gases such as nitrogen, neon, and argon are puffed which can dissipate heat through radiation farther away from the divertor. In the presence of such radiative dissipation, the plasma reaching the divertor reduces, effectively reducing the total ion flux which impinges on the divertor. This phenomenon is known as detachment onset as wetted surface by plasma is reduced. When only part of the surface is wetted, the plasma is said to be partially detached, while if the ion flux is almost completely stopped with higher neutral gas pressure, it is said to be fully detached.

It is important though to keep the amount of impurity gases injected into the vessel to a minimum as higher gas injection eventually leads to more impurity reaching in the pedestal region of the plasma. This can lead to rapid cooling which can collapse H-mode and could also lead to disruption of the plasma confinement. Such sudden loss of plasma confinement can cause damage to the plasma facing components. Thus, it is important to carefully control the amount of impurity injected to keep the divertor cool while not contaminating the core plasma too much.

There are two key ways to control the heat flux reaching the divertor. First is to control the radiated power from the SOL region to maintain optimum dissipation of heat before it reaches the divertor. This has been successfully demonstrated in various machines: using the bolometer chords in diverotor region in Alcator C-Mod[6], JT-60U[7], ASDEX Upgrade[8] and DIII-D[9], using AXUV diodes in EAST[10], using VUV N VII line emission in JET[11], and using C-III emission radiation front measured using MANTIS in TCV[12].

The second way is to control the degree of plasma detachment from divertor target plates. This has been demonstrated widely in several machines as well: using divertor plate temperature measurements with surface thermocouples in Alcator C-Mod[13], using surface elctron temperature measurements with triple-tip Langmuir probes in EAST[14], using ion saturation current measurements from embedded Langmuir probes in

*Corresponding author

Email address: guptaa@fusion.gat.com (Anchal Gupta)

JET[15], and EAST[16]. In KSTAR, the ion saturation current measurements along with core electron density, injected power, and local magnetic field were used to calculate a derived control variable, A_{frac} , which was used to control the detachment[17]. This technique has the added benefit that the rollover ion saturation current does not need to be calculated or estimated prior to the shot and thus this technique has the potential for wider applicability in different scenarios and other machines. In this work, we have re-used this technique in our experiments at KSTAR with tungsten divertor to test the robustness of this control variable in presence of high-Z contamination from tungsten.

In this work, we have also tested a new technique that uses a machine-learning-based surrogate model, DivControlNN[18]. This model integrates measurements from several realtime inputs to run through a large database of 2D UEDGE simulations and provide a realtime estimate of the heat flux reaching the divertor plates along with several other key plasma parameters upstream in SOL and at the two divertors. We tested a prototype of this model with training and input limitations in KSTAR and demonstrated detachment control for the first time using such a surrogate model. This paves way for utilizing such models in future reactors that will have a very limited set of sensors available for control systems.

This paper is organized as following. In Sec.2, we describe the experimental setup and the definition of different control variables used for detachment control. In Sec.3, we describe our experimental shots used for identifying the system and using the fitted plant model to tune a PI controller using frequency response for closed-loop stability analysis and optimization. In Sec.4, we show the results of our detachment control attempts. And finally, in Sec.5, we discuss our results, the possible improvements we can make in future, and other interesting contemporary work and ideas in the field of detachment control.

2. Experimental setup and control variables

The experiment was conducted on standard single lower null H-mode plasma profile with reference shot KSTAR # 35851 with the equilibrium profile as shown in Fig.1. The plasma shaping steps commenced by 7s and the shot was programmed for flat-top upto 17s providing 10s long window for detachment control experiment. For heat flux control, N₂ gas puffing was used. The heat flux control variable was tested with several different inputs.

First, we utilized previously developed A_{frac} [17], which is defined as the ratio of measured ion saturation current to modeled (using 2PM[19]) ion saturation current assuming fully attached plasma. A_{frac} is a convenient choice of control variable which is easily available in most tokamaks and allows for cross comparison among machines. If the strike point on the divertor tile is fixed in position well enough by the shape control system, a single close-by langmuir probe is enough to provide the ion saturation current required for A_{frac} calculation. However, if the strike point control is not good enough, or if it is required to leave it as a free variable to allow for controlling other parameters in the shape control loop (as was the case in

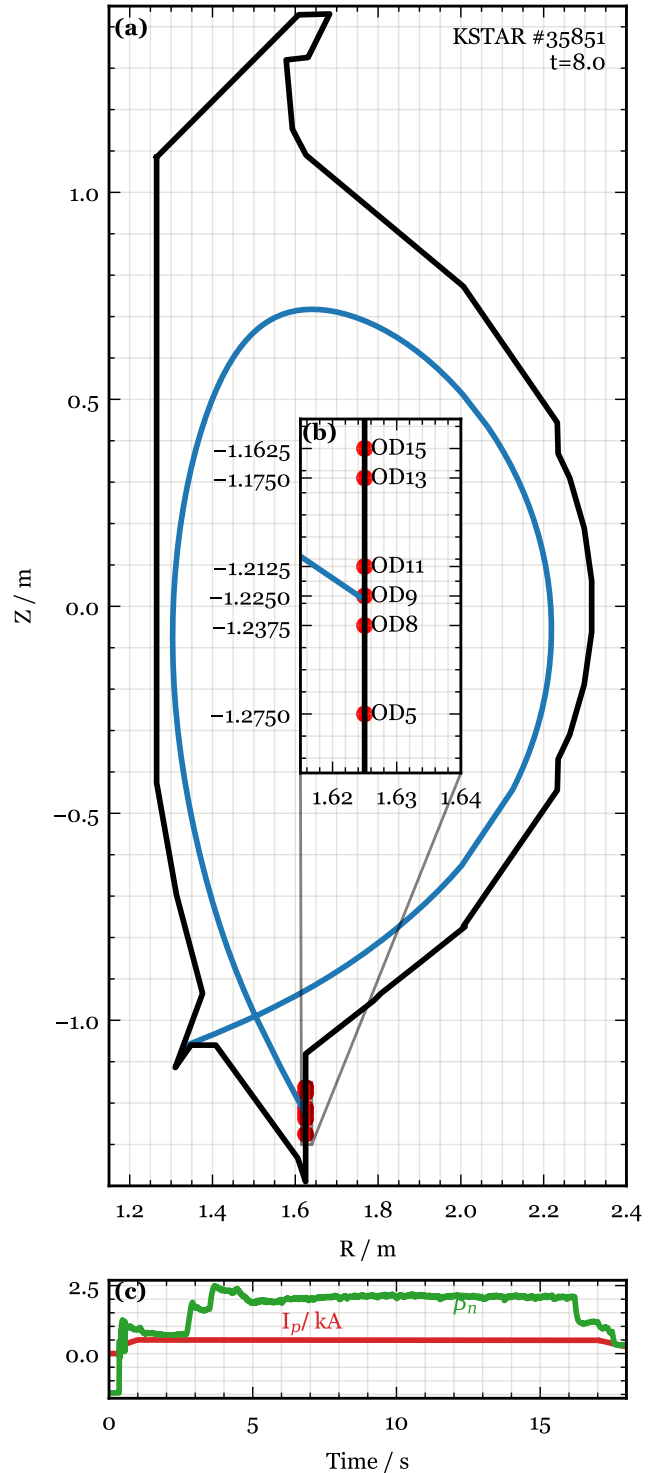


Figure 1: Reference shot # 35851. (a) Showing last closed flux surface at t=8 seconds. The magnetic shape control was programmed to keep X point fixed which provided a sufficiently stable strike point on the realtime Langmuir Probe array. (b) Zoomed-in locations of realtime Outer Divertor (OD) Langmuir probes. (c) Plasma current (I_p) and β_n for reference shot.

our experiments), then it is required to estimate the true ion saturation current through measurements made by an Langmuir probe array. In our experiments, we chose the peak value from

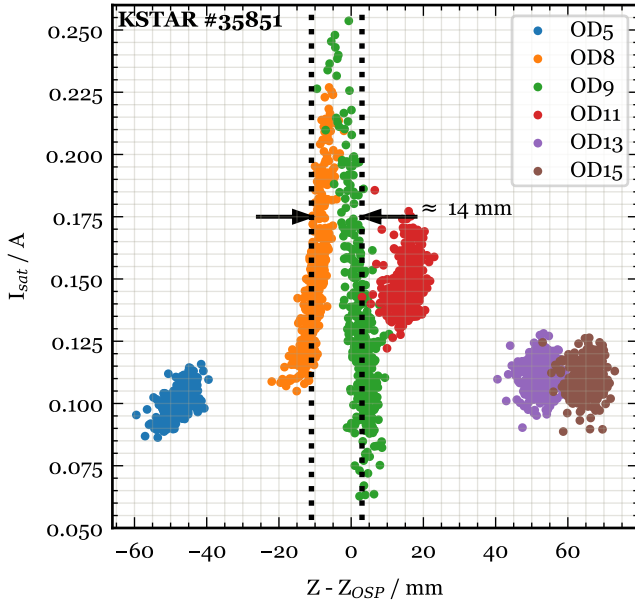


Figure 2: Strike point width estimation for reference shot # 35851. the raw data from langmuir probe array has been filtered by 8th order Butterworth filter ith cut-off frequency of 20 Hz and then down sampled to 40 Hz. For each data point on this plot, the x-axis position is calculated by subtracting the outer strike point (OSP) position reported by EFIT from the probe's Z coordinate.

the langmuir probe array as the input to ion saturation current at strike point. Fig.2 plots the data from this langmuir probe array for our reference shot. The horizontal axis in this figure has been referenced from the EFIT reported outer strike point (OSP) position. Thus, this figure shows the spread of ion saturation current profile across the strike point. Here, we see that the striek point is closer to OD8 and OD9 with a peak ion saturation current value of roughly 0.25 A at the strike point position. We estimate the width of the ion saturation current profile at half the maximum value referenced to the baseline value of 0.1 A measured by far away probes, giving approximately at least a 14 mm wide profile. This ensures that the langmuir probe array as shown in Fig.1 would always have atleast one probe that can confidently measure the ion saturation current for the strike point when the strike point is within the closely placed probes, OD8, OD9, and OD11.

Langmuir probes would not be able to survive high heat flux in burning plasma future reactors. In general, such reactors would be severely limited in the number of realtime sensors available for control systems because of high neutron fluence and heat flux in vacuum vessel, and thus alternate control variables need to be searched for. Towards this goal, we tested a prototype of a machine-learning-based surrogate model of 2D UEDGE, DivControlNN. The employed version of DivControlNN is trained on $\approx 70,000$ 2D UEDGE simulations of KSTAR. The training dataset scanned core electron density ($1.08 \times 10^{19} - 6.62 \times 10^{19} \text{ m}^{-3}$), plasma current (600 – 800 kA), injected total power through NBI and ECH (1 – 8 MW), impurity fraction with respect to Deuterium density (0 – 0.04), and scaling of diffusion coefficient profile with a factor (0.6 –

2). The diffusion coefficient profile is assumed for a typical H-mode shot which can be scaled as an input to the model. This provided a widely applicable surrogate model which gives steady state values of heat flux, ion saturation current, and electron temperature along the two divertors, electron density and temperature at upstream point of midplane, and total radiated power, power fraction radiated from divertor, and peak radiation power location in the poloidal cross-section of the device. The model generates output within 10% error from the 2D UEDGE output.

DivControlNN is orginially developed and trained using python's TensorFlow package and consists of two different models working in tandem. The first is a multi-modal beta-variational autoencoder[20] model to compress various quantities of interest coming from synthetic diagnostics on 2D UEDGE database into a latent space representation. The second stage is a multi-layer perceptron (MLP) model that maps the inputs of the 2D UEDGE simulations (which also form the inputs to the overall surrogate model). During inference operation, the MLP model first maps the inputs to the latent space and the decoder network from the autoencoder then decodes the latent space into useful outputs. While python is the industry choice for developing and training such models, it can not be used for real-time inference purposes such as our use case. We converted the python model into a pure C code using a keras2c[21] package which is developed for generally converting such neural networks into real-time compatible C codes. The generated C code runs an inference operation in about 160 μs on Intel® Core™ i7-6600U CPU @ 2.60GHz while we saw speed up of upto 18 μs per inference on Apple® M2™ Pro. The real-time PCS in KSTAR runs it's divertor control categories in a 5 μs clock cycle CPU, so we ran DivControlNN in a separate 1 ms clock-cycle CPU ensuring enough runtime for it along with other process in that CPU. This was still more than sufficient for our control purposes which anyways can not control faster than few 10s of Hz due to system response time and gas actuation speed.

This preliminary model, however, has been trained on 2D UEDGE simulations of KSTAR with carbon divertor and carbon as the sole impurity species. So it does not reflect the same Tungsten divertor system in which it was tested. There were several other limitations to the realtime input provided to the model. There was no reliable input for impurity fraction in plasma and we created an adhoc gas accumulation model which estimated impurity fraction by taking ratio of total puffed impurity with total puffed Deuterium gas with estimated decay rates to model the effect of pumping and wall adsorption. Additionally at KSTAR, the total input power from NBI and ECH sources is not completely available in realtime PCS and we had to input a feedforward signal matching the programmed rate of some sources that got summed with the other sources whose power was avaialble in realtime. Finally, the diffusion coefficient scaling factor was set to 1.0 for loack of any better realtime information on it. Despite these limitations, we attempted to use this model as a preliminary test for using such a surrogate model in realtime and identify major obstacles before testing an improved and more relevant version in future.

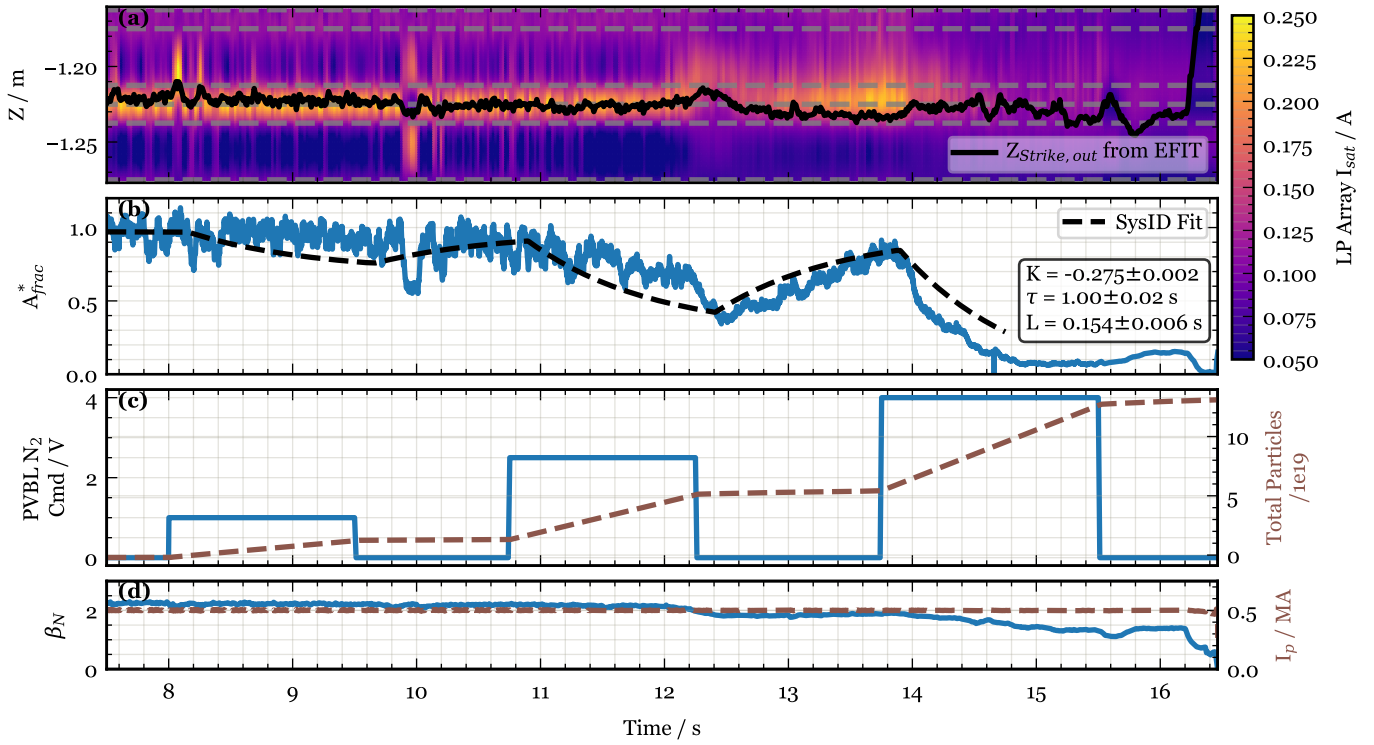


Figure 3: System identification shot # 35853. (a) Shows the measured ion saturation current by realtime Langmuir Probe array at locations marked by grey dashed lines. The data has been interpolated spatially using cubic spline interpolation. The black curve shows the post-shot calculated strike point position on outer divertor using EFIT. (b) Shows the A_{frac} calculated from peak value among the Langmuir probe array. The dashed black line shows the system identification fit on this data. (c) Left axis: Shows the N_2 gas command steps sent for system identification. Right axis: Shows the cummulative N_2 gas particles injected into the vessel. (d) Left axis: Shows β_N . Right axis: Shows the plasma current (I_p). * Note: A_{frac} for this shot was not calibrated properly and the raw data reported 2 times the value. We fixed this factor after this shot and this figure shows the corrected value.

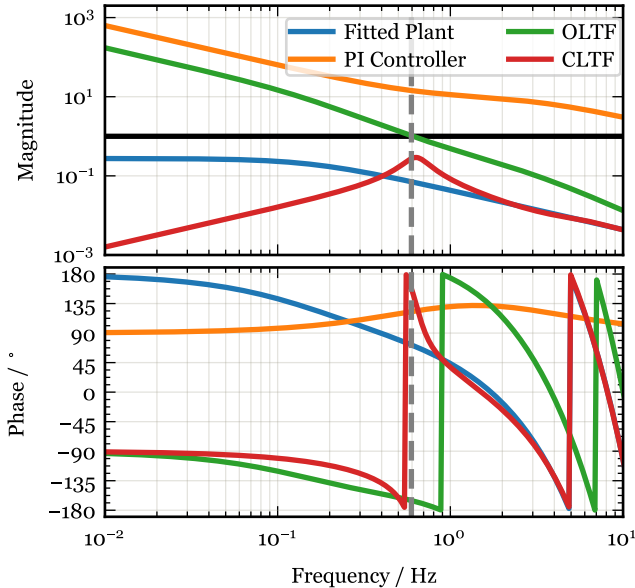


Figure 4: Closed loop transfer function analysis of the system using A_{frac} output with chosen PI controller with gains: $K_p = -10.0$, $T_i = 253.0$ ms, and $\tau_s = 50.0$ ms. The dashed grey verticle line shows the unity gain frequency (UGF) of the system.

3. System identification and Controller Tuning

Before we attempted detachment control experiments, we took two system identification shots. The data from first system identification shot # 35853 is shown in Fig.3. In this shot, we puffed in N_2 gas in steps of 1.0 V, 2.5V, and 4.0 V with puff duration fo 1.5s each. A corresponding response was seen in A_{frac} but with a delay. We later confirmed from post-shot EFIT data that the strike point was indeed within the realtime Langmuir Probe array and thus our A_{frac} calculation was valid. We fitted the measured data with a simple first order plant model of gain K , time constant τ , and time delay L given by:

$$G(s) = \frac{K}{\tau s + 1} e^{-Ls} \quad (1)$$

The fit resulted in identified model with $K = -0.275 \pm 0.002$, $\tau = 1.00 \pm 0.02$ s, and $L = 0.154 \pm 0.006$ s. The fit is shown in Fig.3b. Note that only the part of time series data that was used in fit is shown for the fitted curve. This fit was performed in the inter-shot interval during the experiment and has not been improved or modified after the experiment.

The controller gains were chosen by visualing closed loop transfer function (CLTF) of the system with chosen PI gains as shown in Fig.4. Here, the frequency domain response of the plant model ($G(s)$) and PI controller ($T_{PI}(s)$) are plotted

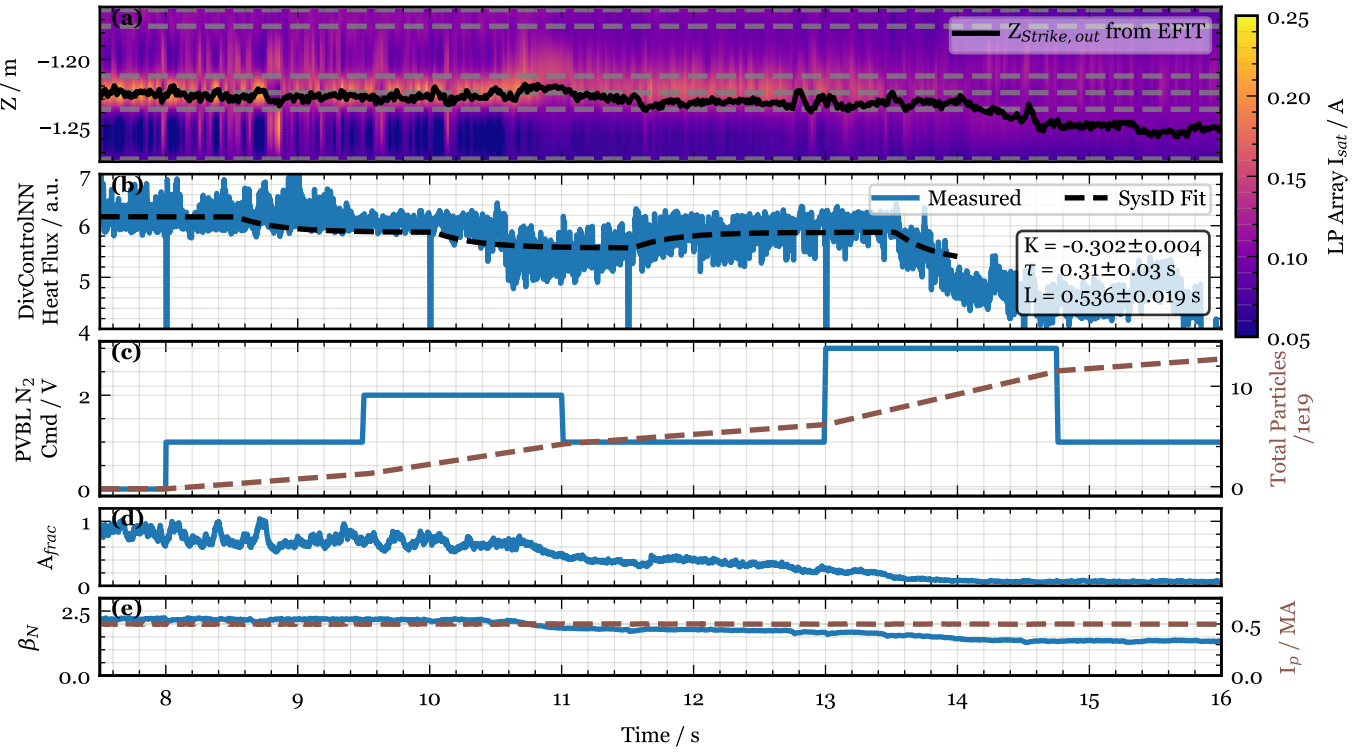


Figure 5: System identification shot # 35854. (a) Shows the measured ion saturation current by realtime Langmuir Probe array at locations marked by grey dashed lines. The data has been interpolated spatially using cubic spline interpolation. The black curve shows the post-shot calculated strike point position on outer divertor using EFIT. (b) Shows the heat flux at outer divertor calculated by DivControlNN. The dashed black line shows the system identification fit on this data. (c) Left axis: Shows the N₂ gas command steps sent for system identification. Right axis: Shows the cummulative N₂ gas particles injected into the vessel. (d) Shows the A_{frac} calculated from peak value among the Langmuir probe array. (e) Left axis: Shows β_N. Right axis: Shows the plasma current (I_p).

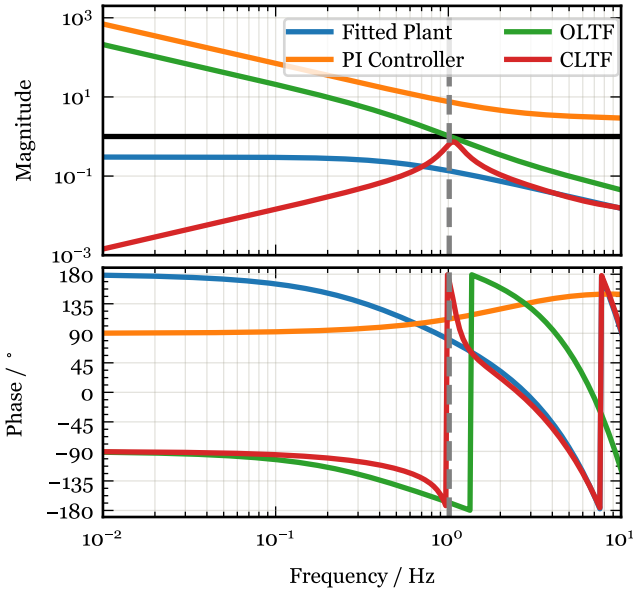


Figure 6: Closed loop transfer function analysis of the system using DivControlNN heat flux at outer divertor output with chosen PI controller with gains: K_p = -3.0, T_i = 68.5 ms, and τ_s = 5.0 ms. The dashed grey verticle line shows the unity gain frequency (UGF) of the system.

together. When connected in series, this forms the open loop transfer function (OLTF) of the system ($O(s) = G(s)T_{PI}(s)$). The frequency where OLTF becomes 1.0 is called unity gain frequency (UGF). Phase margin is defined as the additional phase delay at UGF that would make the system unstable by taking it to -180°. Additionally, we also define delay margin as the additional actuation delay that would make UGF unstable. The CLTF is then calculated by solving the loop algebra in laplace domain:

$$C(s) = \frac{G(s)}{1 + O(s)} \quad (2)$$

Because of the large delay, we chose to not use derivative gain. The goal of tuning was to push UGF as high as possible (0.59 Hz) while keeping a reasonable phase margin (14.8 °) and margin for any additional actuation delay (69 ms). This resulted in controller settings as: K_p = -10.0, T_i = 253.0 ms, and τ_s = 50.0 ms, where K_p is proportional gain, T_i is integral time, and τ_s is presmothing time constant. This is still a very aggressive choice of controller, but given that the system identification fit gave an unexpectedly high value of response time τ = 1s probably due to too much noise during low step inputs, we decided to go ahead with this controller choice. The resulting PI controller transfer function is given by:

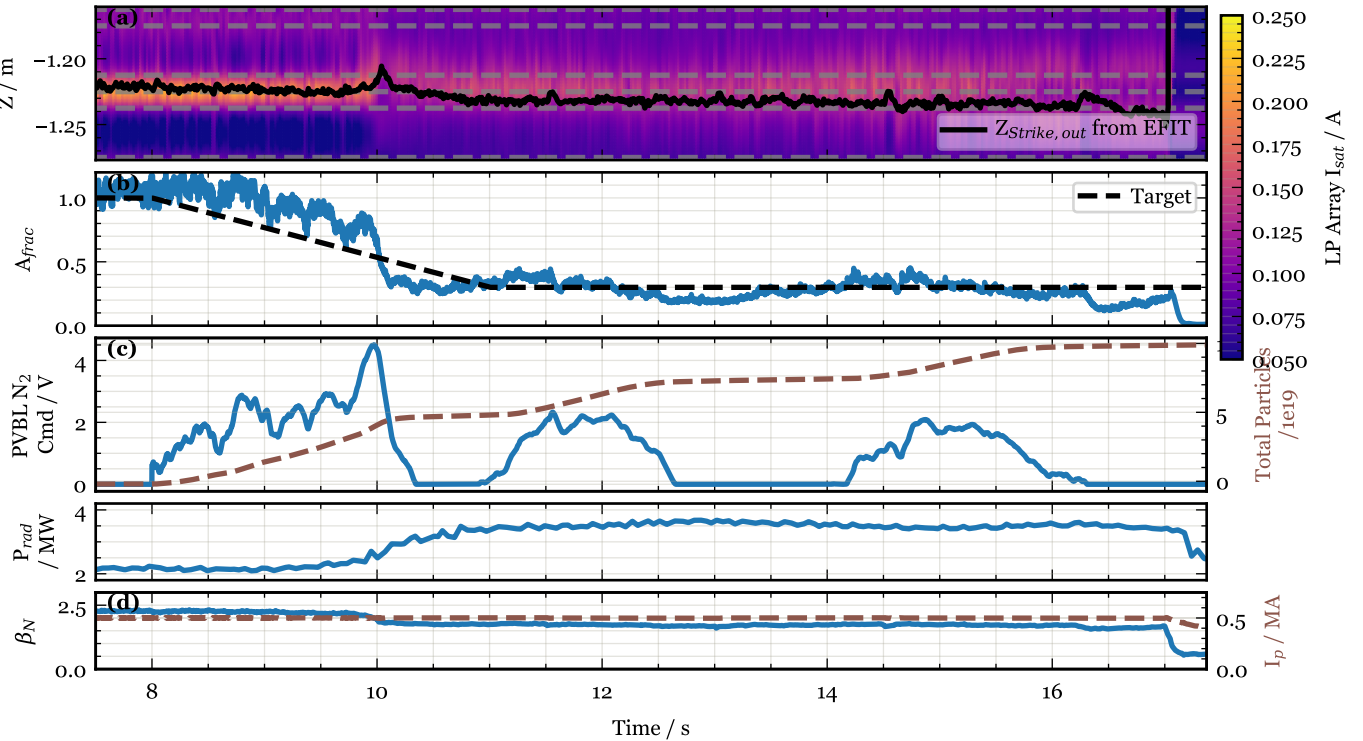


Figure 7: Detachment control shot # 35857 using A_{frac} -controller. (a) Shows the measured ion saturation current by realtime Langmuir Probe array at locations marked by grey dashed lines. The data has been interpolated spatially using cubic spline interpolation. The black curve shows the post-shot calculated strike point position on outer divertor using EFIT. (b) Shows the A_{frac} calculated from peak value among the Langmuir probe array. The dashed black line shows the target provided to the controller to follow. (c) Left axis: Shows the N_2 gas command steps sent for system identification. Right axis: Shows the cummulative N_2 gas particles injected into the vessel. (d) Total radiated power measured by Infra-Red Video Bolometer. (e) Left axis: Shows β_n . Right axis: Shows the plasma current (I_p).

$$T_{PI}(s) = K_p \left(\frac{1}{T_i s} + 1 \right) \frac{1}{1 + \tau_s s} \quad (3)$$

Unfortunately, the surrogate model was not configured properly in this system identification shot due to technical errors, so we repeated a system identification but this time we decided to keep the nitrogen valve in constant open position, to look for any deviation in the behavior. The data from this second system identification shot is shown in Fig.5. Despite all the limitations of DivControlNN as listed earlier, we still saw a good correlation in the DivControlNN heat flux output at outer divertor with the injected gas as seen in Fig.5b. This is validated by estimated A_{frac} in Fig.5d showing an increase in detachment level as the predicted output heat flux decreases. The strike point was maintained within the realtime Langmuir probe array (Fig.5a) validating the output of A_{frac} . Note that we did not yet calibrate the DivControlNN model with any experimental data, so we treat the output as arbitrary units and later attempted to control the detachment with estimated changes to this arbitrary output.

We again fitted this system with a first order system with delay as described in Eq.1. The fit resulted in identified model with $K = -0.302 \pm 0.004$, $\tau = 0.31 \pm 0.03$ s, and $L = 0.536 \pm 0.019$ s. The fit is shown in Fig.5b. Here as well, the fitting shown was performed during the experiment in the inter-shot interval and has not been modified or optimized later. The time domain in

which fitting curve is shown is the data where the system was fitted. Admittedly, this fit was not very good and we did not believe the large lag value to be accurate. So for the purpose of tuning the controller, we arbitrarily set the system lag value to 100 ms. The controller gains were chosen by visualing CLTF of the system with chosen PI gains as shown in Fig.6 and following the same procedure as we described for A_{frac} -controller tuning. The resulting controller settings were: $K_p = -3.0$, $T_i = 68.5$ ms, and $\tau_s = 5.0$ ms creating controller given by Eq.3. Here, we estimated to achieve a UGF of 1.01 Hz, phase margin of 11.9° , and delay margin of 33 ms. This controller was also very aggressive, but we decided to go ahead with this controller choice given the limitations of the system identification fit and lack of time for further analysis in between the allotted run time to our experiment.

4. Results

Utilizing the controllers tuned in Sec.3, we attempted detachment control experiments. First, we used A_{frac} -controller in KSTAR # 35857 with results shown in Fig.7. As can be seen in Fig.7a, the strike point remained within the realtime Langmuir probe array giving validity to the A_{frac} signal shown in Fig.7b. Here, we can see that the controller was successful in closely following the target provided to it completing

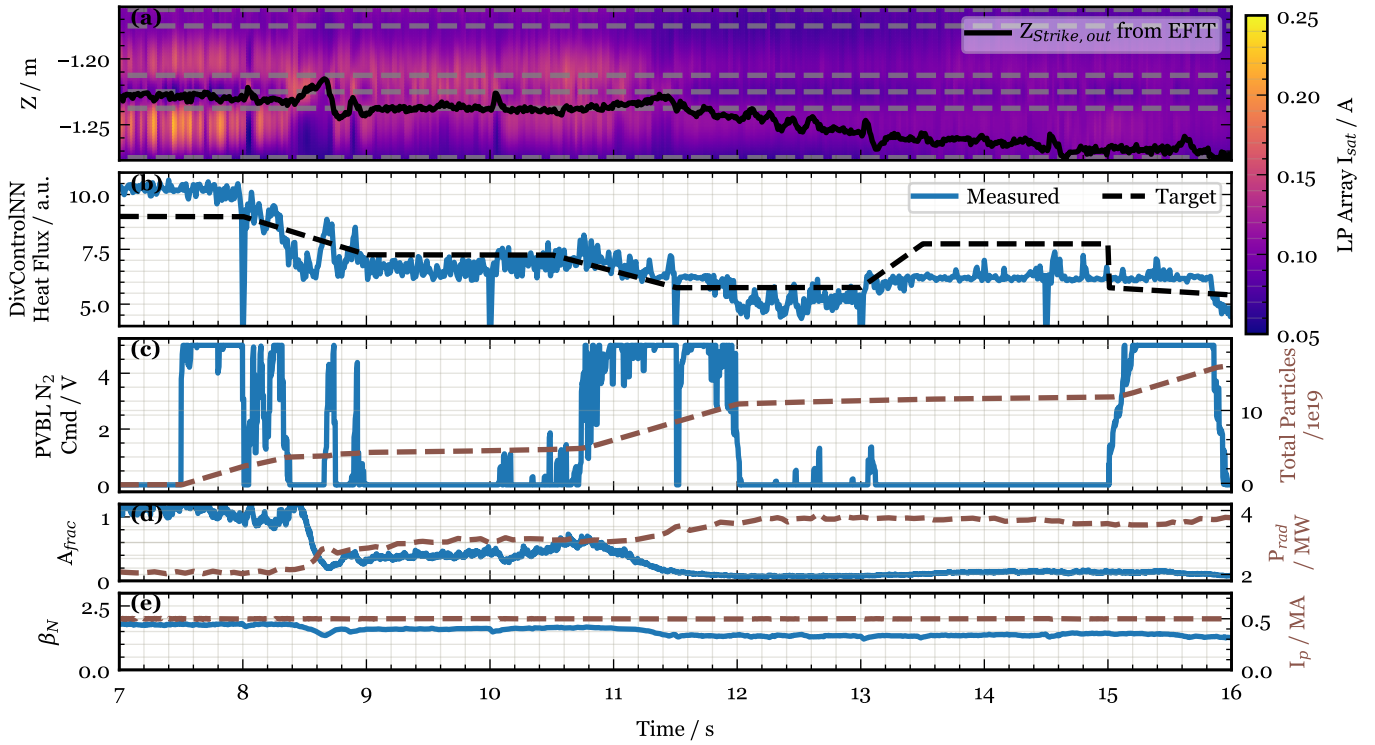


Figure 8: Detachment control shot # 36161 using DivControlNN heat flux at outer divertor. (a) Shows the measured ion saturation current by realtime Langmuir Probe array at locations marked by grey dashed lines. The data has been interpolated spatially using cubic spline interpolation. The black curve shows the post-shot calculated strike point position on outer divertor using EFIT. (b) Shows the heat flux at outer divertor calculated by DivControlNN. The dashed black line shows the target provided to the controller to follow. (c) Left axis: Shows the N_2 gas command steps sent for system identification. Right axis: Shows the cummulative N_2 gas particles injected into the vessel. (d) Left axis: Shows the A_{frac} calculated from peak value among the Langmuir probe array. Right axis: Total radiated power measured by Infra-Red Video Bolometer. (e) Left axis: Shows β_n . Right axis: Shows the plasma current (I_p).

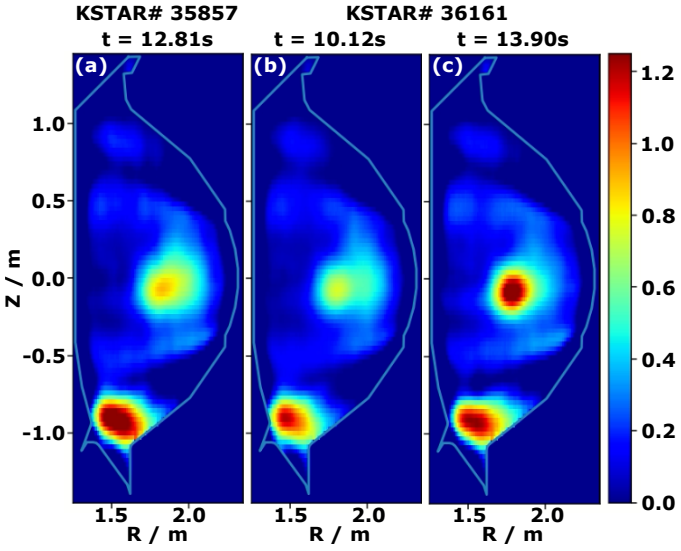


Figure 9: KSTAR IRVB measured radiated power density (a.u.) inverted into 2D cross-section. (a) KSTAR # 35857 at 12.81s at the peak of total radiated power. (b) KSTAR # 36161 at 10.12s before the second impulse of gas between 10.8s to 12s. (c) KSTAR # 36161 at 13.90 after the last gas impulse.

the pre-programmed shot length to the end. It is also evident that the aggressive control strategy was good and did not re-

sult in any long sustained oscillations while providing a quick response to the changing target value. This further validated, that A_{frac} controller strategy first devised in Ref.[17] is a viable option for detachment control even with Tungsten divertor in KSTAR.

Since A_{frac} controller has been demonstrated in the past as well, we decided to utilize remaining allotted runtime on KSTAR to test the DivControlNN prototype based controller. Fig.8 shows the results from shot # 36161 where we deployed this controller. An immediate issue was seen with DivControlNN output that the intial heat flux calculation had a starting value than we saw in reference shots and system identification shot # 35854. Because of this, when the controller turned on at 7.5s, the large error resulted in railing of gas command output which resulted in too much N_2 injected into the system. While this quickly brought down the measured signal, it also resulted in a large overshoot and probably created power starvation in the core plasma. This is evident from the system behavior in the following seconds where the calculated heat flux output did not rise much even though impurity injection was stopped. In the nest rampdown of target from 10.5s to 11.5s, more impurity was injected as we tuned an aggresive controller. It can be seen from A_{frac} in Fig.8d that the system reached into deep detachment by this point and the ion saturation current measurements (Fig.8a) became unreliable beyond 11s. This is why the heat

flux did not naturally recover even when the target was lifted up between 13s to 15s. There is no surprise with the fact that using an uncalibrated output can result in bad set target values.

Post-shot data analysis discovered further issues in our operation of the DivControlNN model. The impurity fraction calculation as mentioned in 2 malfunctioned and sent a constant zero input to the model. Thus the model was unable to respond to large amounts of impurity that were injected into the system and was only relying on data from line integrated core electron density and plasma current as realtime inputs. Despite these limitations, this preliminary test sheds light on the potential of using such a surrogate model based controller for detachment control in future reactors.

5. Discussion

In this paper, we described re-using A_{frac} as a reliable control variable for detachment control provided that realtime ion saturation current measurements are available from the Langmuir probes and the strike point is controlled good enough that such an array can be used to calculate A_{frac} . I can be seen from panels (a) and (c) in Fig.3, Fig.5, and Fig.8 that when the total injected impurity amount crosses a rough threshold of about 1×10^{20} particles, the plasma shape starts to rotate such that strike point on outer divertor starts drifting downwards even though the X-point is held in place by the magnetic shape control system. Thus, A_{frac} controller is best suited with a outer strike point control system commissioned on the device which was not the case for the KSTAR experimental campaign in which we tested these controllers.

Although, langmuir probes might not be able to survive future burning plasma experiments, sacrificial probes can still be used in commissioning controllers based on other control variables in such devices given the success and reliability of this control method being demonstrated in several devices so far [NEEDCITE]. The good results from A_{frac} controller as seen in Fig.7 could also motivate further research in similar biased electrode measurement methods of SOL plasma such as biased divertor plates [NEEDCITE] and biased ring electrodes [NEEDCITE].

We were also able to perform a preliminary test on using DivControlNN output as a control variable for detachment control. This is an important step in the direction of achieving detachment control in future burning plasma reactors which would have very limited means of measuring the detachment level. We have identified critical weak points in the prototype of DivControlNN and the control infrastructure required to utilize this model, and we are working on improving these aspects for future tests. This further motivates focus on training surrogate models on wider set of input parameters and plasma scenarios for possible use in other control systems as well as an alternate way to provide fast diagnostic outputs in the control room during experiments for quick decision making.

Another major focus of future experiments would be to use noble gases in detachment control as N₂ while being optimum in cooling the SOL plasma is not allowed in burning plasma

devices due to formation of tritiated ammonia that poses radioactive dangers. We are in the process of testing Ne and Ar as alternate colloidal gases. More widely, there has been recent interest in using pellets for impurity injection for detachment control to reduce the large lag time and response time associated with gas puffing. Another alternative is dropping the impurity in the form of solid powder, such as Boron, although the investigation on its use for this purpose is still in preliminary phase and poses additional challenges in terms of long lag time due to free fall and accumulation of unused powder in the device.

CRediT authorship contribution statement

Declaration of competing interest

The authors declare that they have no known competing financial interests or personal relationships that could have appeared to influence the work reported in this paper.

Acknowledgements

This material is based upon work supported by the U.S. Department of Energy, Office of Science, Office of Fusion Energy Sciences, under Awards DE-SC002340, and DE-AC52-07NA27344.

Disclaimer

This report was prepared as an account of work sponsored by an agency of the United States Government. Neither the United States Government nor any agency thereof, nor any of their employees, makes any warranty, express or implied, or assumes any legal liability or responsibility for the accuracy, completeness, or usefulness of any information, apparatus, product, or process disclosed, or represents that its use would not infringe privately owned rights. Reference herein to any specific commercial product, process, or service by trade name, trademark, manufacturer, or otherwise, does not necessarily constitute or imply its endorsement, recommendation, or favoring by the United States Government or any agency thereof. The views and opinions of authors expressed herein do not necessarily state or reflect those of the United States Government or any agency thereof.

References

- [1] N. Holtkamp, [An overview of the iter project](#), Fusion Engineering and Design 82 (5) (2007) 427–434, proceedings of the 24th Symposium on Fusion Technology.
- [2] A. J. Creely, et al., [Overview of the sparc tokamak](#), Journal of Plasma Physics 86 (5) (2020) 865860502.
- [3] T. Eich, et al., [Scaling of the tokamak near the scrape-off layer h-mode power width and implications for iter](#), Nuclear Fusion 53 (9) (2013) 093031.

- [4] R. Pitts, et al., [Physics basis for the first iter tungsten divertor](#), Nuclear Materials and Energy 20 (2019) 100696.
- [5] S. Brezinsek, et al., [Erosion, screening, and migration of tungsten in the jet divertor](#), Nuclear Fusion 59 (9) (2019) 096035.
- [6] J. A. Goetz, et al., [High confinement dissipative divertor operation on alcator c-mod](#), Physics of Plasmas 6 (5) (1999) 1899–1906.
- [7] N. Asakura, et al., [Investigations of impurity seeding and radiation control for long-pulse and high-density h-mode plasmas in jt-60u](#), Nuclear Fusion 49 (11) (2009) 115010.
- [8] A. Kallenbach, et al., [Optimized tokamak power exhaust with double radiative feedback in ASDEX Upgrade](#), Nucl. Fusion 52 (2012) 122003.
- [9] D. Eldon, et al., [Advances in radiated power control at diii-d](#), Nuclear Materials and Energy 18 (2019) 285–290.
- [10] K. Wu, et al., [Achievement of radiative feedback control for long-pulse operation on east](#), Nuclear Fusion 58 (5) (2018) 056019.
- [11] G. Maddison, et al., [Demonstration of real-time control of impurity seeding plus outboard strike-point sweeping in jet elmy h-mode plasmas](#), Nuclear Fusion 51 (8) (2011) 082001.
- [12] T. Ravensbergen, et al., [Real-time feedback control of the impurity emission front in tokamak divertor plasmas](#), Nature Communications 12 (2021) 1105.
- [13] D. Brunner, et al., [Surface heat flux feedback controlled impurity seeding experiments with alcator c-mod's high-z vertical target plate divertor: performance, limitations and implications for fusion power reactors](#), Nuclear Fusion 57 (8) (2017) 086030.
- [14] D. Eldon, et al., [An analysis of controlled detachment by seeding various impurity species in high performance scenarios on diii-d and east](#), Nuclear Materials and Energy 27 (2021) 100963.
- [15] C. Guillemaut, et al., [Real-time control of divertor detachment in h-mode with impurity seeding using langmuir probe feedback in jet-iter-like wall](#), Plasma Physics and Controlled Fusion 59 (4) (2017) 045001.
- [16] Q. Yuan, et al., [The first implementation of active detachment feedback control in east pcs](#), Fusion Engineering and Design 154 (2020) 111557.
- [17] D. Eldon, et al., [Enhancement of detachment control with simplified real-time modelling on the KSTAR tokamak](#), Plasma Physics and Controlled Fusion 64 (7) (2022) 075002.
- [18] B. Zhu, et al., [Latent space mapping: Revolutionizing predictive models for divertor plasma detachment control](#), In Preparation.
- [19] A. W. Leonard, [Plasma detachment in divertor tokamaks](#), Plasma Physics and Controlled Fusion 60 (4) (2018) 044001.
- [20] I. Higgins, et al., [beta-VAE: Learning basic visual concepts with a constrained variational framework](#), in: International Conference on Learning Representations, 2017.
- [21] R. Conlin, A. Gupta, [keras2c \(forked from plasmacontrol/keras2c\). general python keras model to real-time c converter.](#), in: Github with GNU Lesser GPL 3 License, 2024.